TRANSPORT
ISSN 1648-4142 / eISSN 1648-3480
2015 Volume 30(2): 217–232
doi:10.3846/16484142.2015.1051108

THE DYNAMIC BEHAVIOUR OF A WHEEL FLAT OF A RAILWAY VEHICLE AND RAIL IRREGULARITIES

Marijonas Bogdevičius[1], Rasa Žygienė[2], Stasys Dailydka[3], Vilius Bartulis[4], Viktor Skrickij[5], Saugirdas Pukalskas[6]

[1, 2, 4, 5]*Dept of Transport Technological Equipment, Vilnius Gediminas Technical University, Lithuania*
[3]*Dept of Railway Transport, Vilnius Gediminas Technical University, Lithuania*
[6]*Dept of Automobile Transport, Vilnius Gediminas Technical University, Lithuania*

Submitted 7 July 2014; resubmitted 16 December 2014, 9 May 2015; accepted 10 May 2015

Abstract. The article examines a mathematical model for the system 'Railway Vehicle Wheel–Track' that allows examining the interaction between a wheel flat and a rail in the vertical plane. The dynamics of the railway track is described using the finite element method while that of the soil and vehicle is expressed applying discrete elements. The model is used for assessing physical and mechanical properties, the roughness of the wheel, rail surface and their geometry. The analysis of the dynamic system 'Railway Vehicle Wheel–Track' has been conducted. In accordance with the revised method, forces arising from contact between the wheel flat and the rail are possible to be determined in a more precise way. The article presents and analyses the results of a mathematical experiment on this system.

Keywords: rail; wheel flat; defects; contact; dynamics; numerical method.

Introduction

Along the evolving technology, the number of the means of transport is increasing, traffic is getting more intense worldwide and rail traffic is growing. Therefore, special attention is paid to railway vehicles, infrastructure maintenance and traffic safety. In the case of the interaction between a moving train wheel and the rail, the forces resulting from their physical condition, metal stress (Ahmetzyanov 2003), deformation, noise, etc. are formed. The article studies the effects of various working conditions on the surface of the rail (Donzella *et al.* 2009). Axles can move laterally because of the forces resulting from the interaction between the wheel and the rail, while a lateral displacement can lead to wheel or track alterations.

A number of models for wheel–rail interference have been developed. However, when formulating wheel–rail issues and setting targets, the scientist presents (Yazykov 2004; Uzzal 2012; Wu, Thompson 2001; Torstensson *et al.* 2011) different solutions to this problem. A vertical non-linear Hertzian contact model based on research into the behaviour of two moving cylinders is widely used for investigation of the wheel–rail interaction. The assumption that a very small contact area is observed inside the contact of two bodies has been made.

For dealing with the problems of railway wheel–rail interaction, finite element models have been designed (Recuero *et al.* 2011). Numerical models (Wasiwitono *et al.* 2007; Zhu *et al.* 2007; Wu, Thompson 2001; Bezin *et al.* 2009) allow predicting the dynamic interaction of the 'wheel–rail–soil' system. Vibrations arising in the system are divided into finite elements.

Dynamic models allow to predict the state of the system or the influence of a dynamic system in the event of having a variety of factors. When performing tests on dynamic behaviour, the railway track and vehicle change, and the movements and degrees of freedom are taken into account. A number of dynamic models having various degrees of freedom, taking into account different dynamic characteristics and various parameters, are presented. The forces arising from the wheel–rail interaction (Pombo *et al.* 2007) are calculated referring to dynamic movement and evaluating tangential forces under normal forces and velocity between two moving bodies using the Kalker's (1979) linear theory, heuristic non-linear methods and Polach's (2000) formulation.

Numerical dynamic simulation models are used for researching trains. Many dynamic models are designed to monitor and predict the movement of the means of transportation and contact between the rail and the

Corresponding author: Marijonas Bogdevičius
E-mail: *marijonas.bogdevicius@vgtu.lt*

Taylor & Francis
Taylor & Francis Group

wheel (Zhu *et al.* 2007). In order to reduce the number of the degrees of freedom and decrease simulation time while creating a dynamic system, the simplification of elements to springs–dampers and masses is employed.

Sun *et al.* (2003) is described a dynamic model of a three-dimensional vertical-horizontal multi-body system consisting of a vehicle and the road using Kalker's creep and Hertzian contact methods, including the wheel–rail interaction with a variety of loads.

Railways are systematically inspected during both production and service processes using various non-destructive element testing methods. One of the main indicators characterizing the lifetime of the railway track is its age. A large focus of scientists goes on defects in the railway wheel or rail surface, their measurements, growth monitoring and forecasting (Kasimov 2009; Markov 2004). One of the main evaluation criteria for a defected track are the stress intensity factor, as it can be used for predicting growth in rail defects. Most defects in the railway track are found in the railhead and mainly emerge due to contact stress.

For analysing the status of soil, a system for sleepers and rails (Aursudkij 2007; Herron *et al.* 2009) at a critical load and the impact force of equipment wheels (Kaewunruen *et al.* 2014), a mathematical model has been developed.

The load of the wheel plays an important role in the bending moment of the sleeper; pulse duration is greater, which explains such phenomena as the fracture of sleepers from wheel impact.

Wheel and rail response, due to parametric excitation by the varying dynamic stiffness of a periodically supported rail, has been studied using a spatial quasi-static method (Bogacz *et al.* 1993).

The ground properly laid under the sleeper can improve or help with obtaining the desired features of the upper construction of the track. In order to reduce the forces affecting sleepers, soil stiffness should be reduced, and, in order to minimize the bending moment of the track, stiff soil should be chosen.

The conducted research has concluded that the tie without support increases vibrations, reduces adhesion and is likely to lead to an increase in wheel and rail defects and noise, the risk of load stability and even human life.

Concerning the design of the wheel or rail, there are forces of different extent generated between the wheel and the rail in a connection with potential rail joints and welds, various train speeds, forces of breaking, locking of the wheel and the mass of the car. These forces are able to cause wheel flats of a different size and produce the latter vibrations of the rails and car. Geometrical defects of the wheel and rail are rarely detected at the initial stages of operation; however, these faults increase over time. A number of scientists describe the contact area of the wheel–rail as a point, or define wheel geometry by an analytical function in mathematical models (Barke, Chiu 2005; Bian *et al.* 2013; Kouroussis *et al.* 2011; Nielsen, Abrahamsson 1992; Pieringer *et al.* 2014; Sackfield *et al.* 2006, 2007).

Scientists have researched the time and length history of vehicle mass and displacement acceleration by examining dynamic processes happening inside the contact area (Ferrara *et al.* 2012; Kumar, Rastogi 2009; Uzzal *et al.* 2009; Wang *et al.* 2015; Wasiwitono *et al.* 2007). The spectra of accelerations of the vehicle mass are calculated using discrete Fourier transform (Nielsen *et al.* 2008; Wang *et al.* 2015, Wasiwitono *et al.* 2007).

The analysis of scientific articles showed there was no single method according to which dynamic processes occurring in the interaction between vehicle flats and the track were developed. Each author has preferred different simulation parameters.

The article proposes the revised method for determining forces arising from the contact of the wheel flat and the rail and other characteristics of contact. Geometrical irregularities of the wheel and flat, the unevenness of the rail and the micro-unevenness of the bodies in the contact area are assessed in the revised model. Particular attention is paid to determining the forces arising in the contact of the wheel flat and the rail. The area of contact is divided into a number of intervals at any given time between the bodies in contact. The interval may extend from 1 to 100 μm. At the points of contact, possible short-term intervals between the wheel and the rail are assessed, and therefore, at each time point between the contacting surfaces, the distribution of the load varies.

According to the revised method, velocities of slip, relative longitudinal slip, normal and friction forces and the moment of friction torque forces acting on the wheel are established in the contact area between two surface points in contact at each point in time. Using this information allows determining the average values of those characteristics in the contact area at each point in time.

In regard to the indicated revised method that determines contact force, wheel and rail depreciation problems, loads on the bearing of the wheel and impact on soil can be investigated. The theoretical part deals with the revised method of contact force allowing the determination of forces acting in the contact and characteristics of the contact.

The article is aimed at revealing all stages of the considered issues selected by the scientists and refers to possible ways of solving them.

1. A Vertical Dynamic Model for the Interaction between the Railway Track and the Vehicle

The rail profile is considered as a stochastic function where unevenness parameters of the actual rail are measured. The mathematical model of the wheel and rail contact allows us determining the forces resulting from contact when assessing defects. The carried out investigation is focused on identifying contact forces resulting from the wheel and rail contact under various defects. The mathematical model was created in order to analyse the main defects of the vehicle wheel.

A computational model is composed of a vehicle and the road divided into finite elements. The article

analyses the task of nonlinear dynamics. It is assumed that gaps can occur between two bodies in contact and between the rail and the sleeper. The equations of the system elements are set employing d'Alembert's principle.

The issues of nonlinear dynamics are considered applying the numerical methods of Newton–Raphson and Newmark (1947).

1.1. The System of Equations 'Railway Vehicle Wheel–Track' for the Rail

When studying rail interaction with the wheel–rail and sleepers, it can be assumed that the rail deforms at X in the Z plane and can be evaluated as follows:

- variable characteristics of the rail cross-section (rail unevenness is measured);
- rail interaction with the roadbed as a tough base;
- potential space between the rail and roadbed;
- the length of the rail and the wheel–rail contact and geometrical imperfections in it;
- the impact of axial forces in the rail on stiffness (because of difference in temperature);
- the initial deformation of the rail;
- a gap between the sleeper and the rail.

The dynamics of the rail has been considered applying the finite element method. Two node beam element is used (Fig. 1).

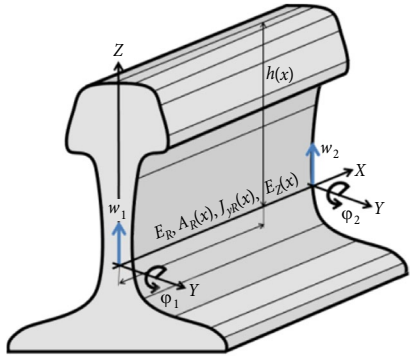

Fig. 1. Parameters for assessing rail unevenness

Displacement w and initial displacement w_0 along the Z axes of the beam finite element are equal to:

$$w = \left[N_w(\xi)\right]\{q_e\};$$

$$w_0 = \left[N_w(\xi)\right]\{w_{0e}\}, \quad (1)$$

where: $\{w_{0e}\}$ is the initial displacement vector; $\{q_e\}$ is a displacement vector; $\left[N_w(\xi)\right]$ is a matrix of shape functions.

The matrix of shape functions equals:

$$\left[N_w(\xi)\right] = \left[1-3\xi^2+2\xi^3 \quad -L_e\xi\left(1-2\xi+\xi^2\right),\right.$$

$$\left. 3\xi^2-2\xi^3 \quad L_e\xi^2\left(1-\xi\right)\right], \quad (2)$$

where: $\xi = \frac{x}{L_e}$ is a local coordinate; L_e is the length of the finite element.

The potential energy of beam finite element L_p consists of the potential energies of bending $E_{p,b}$, tension force $E_{p,T}$ and elastic foundation $E_{p,F}$:

$$E_p = E_{p,b} + E_{p,T} + E_{p,F}, \quad (3)$$

where:

$$E_{p,b} = \frac{1}{2}\int_0^{L_e} E_R J_{yR}(x)\left(\frac{\partial^2 w}{\partial x^2} - \frac{\partial^2 w_0}{\partial x^2}\right)^2 dx =$$

$$\frac{1}{2}\{q_e\}^T\left[K_{1e}\right]\{q_e\} - \{q_e\}^T\{F_{01e}\} + E_{p,b0}, \quad (4)$$

where: E_R is a modulus of rail elasticity; $J_{yR}(x)$ is the axial moment of inertia; $\{F_{01e}\}$, $E_{p,b0}$, $\left[K_{1e}\right]$ is the force vector of finite elements, potential energy evaluating the initial shape of the rail and stiffness matrix respectively:

$$\{F_{01e}\} = \left[K_{1e}\right]\{w_{0e}\};$$

$$E_{p,b0} = \frac{\{w_{0e}\}^T\left[K_{1e}\right]\{w_{0e}\}}{2};$$

$$\left[K_{1e}\right] = \int_0^L \left[\frac{\partial^2 N_w(\xi)}{\partial \hat{\imath}^2}\right]^T \frac{E_R J_{yR}(x)}{L_e^3}\left[\frac{\partial^2 N_w(\xi)}{\partial \hat{\imath}^2}\right] d\xi.$$

The potential energy of the finite element under acting tension force is equal to:

$$E_{p,T} = \frac{1}{2}\int_0^{L_e} F_a\left(\frac{\partial w}{\partial x} - \frac{\partial w_0}{\partial x}\right)^2 dx =$$

$$\frac{1}{2}\{q_e\}^T\left[K_{2e}\right]\{q_e\} - \{q_e\}^T\{F_{02e}\} + E_{p,T0}, \quad (5)$$

where: F_a is tension force; $\{F_{02e}\}$, $E_{p,T0}$, $\left[K_{2e}\right]$ are the force vector of finite elements, potential energy, the stiffness matrix of the finite element under operating axial force respectively,

$$\{F_{02e}\} = \left[K_{2e}\right]\{w_{0e}\};$$

$$E_{p,T0} = \frac{\{w_{0e}\}^T\left[K_{2e}\right]\{w_{0e}\}}{2};$$

$$\left[K_{2e}\right] = \int_0^L \left[\frac{\partial N_w(\xi)}{\partial \xi}\right]^T \frac{F_a}{L_e}\left[\frac{\partial N_w(\xi)}{\partial \xi}\right] d\xi.$$

The potential energy of the finite element lying on the foundation is equal to:

$$E_{p,F} = \frac{1}{2}\int_0^L k_S(x)\left(w(x) - w_0(x)\right)^2 dx =$$

$$\frac{1}{2}\{q_e\}^T\left[K_{3e}\right]\{q_e\} - \{q_e\}^T\{F_{03e}\} + E_{p,F0}, \quad (6)$$

where: $k_S(x)$ is the coefficient of the stiffness of the elastic foundation; $\{F_{03e}\}$, $E_{p,F0}$, $\left[K_{3e}\right]$ are the force vector of the finite element, the potential energy of the finite element, the stiffness matrix of the finite element under the present elastic basis respectively,

$$\{F_{03e}\} = \left[K_{3e}\right]\{w_{0e}\};$$

$$E_{p,F0} = \frac{1}{2}\{w_{0e}\}^T [K_{3e}];$$

$$[K_{3e}] = \int_0^L [N_w(\xi)]^T k_S(x) [N_w(\xi)] L_e d\xi.$$

The damping matrix of the beam finite element of the rail is equal to:

$$[C_e] = \alpha[M_e] + \beta[K_e], \quad (7)$$

where: α, β are optional coefficients; $[M_e]$ is the mass matrix; $[K_e]$ is the stiffness matrix.

Mass matrix of the beam finite element of the rail is equal to:

$$[M_e] = \int_0^1 [N_w(\xi)]^T \rho_R A_R [N_w(\xi)] L_e d\xi, \quad (8)$$

where: ρ_R is rail material density; A_R is the rail cross-section area.

The stiffness matrix is equal to:

$$[K_e] = [K_{1e}] + [K_{2e}] + [K_{3e}]. \quad (9)$$

The load vector of the finite element is equal to:

$$\{F_e\} = \{F_w\} + \{F_{Se}\} + \{F_{contact}\}, \quad (10)$$

where: $\{F_w\}$ is a vector of weight force,

$$\{F_w\} = \int_0^{L_e} [N_w(\xi)]^T q_w L_e d\xi; \quad (11)$$

$\{F_{Se}\}$ is a force vector depending on axial force, bending and an elastic basis of the rail,

$$\{F_{Se}\} = \{F_{01e}\} + \{F_{02e}\} + \{F_{03e}\}; \quad (12)$$

$\{F_{contact}\}$ is a vector of contact force,

$$\{F_{contact}\} = \int_{\xi_a}^{\xi_b} [N_w(\xi)]^T q(\xi) L_e d\xi, \quad (13)$$

where: $q(\xi)$ is a distributed load in the contact area between the rail and the wheel.

The system of equations for the beam finite element of the rail is equal to:

$$[M_e]\{\ddot{q}_e\} + [C_e]\{\dot{q}_e\} + [K_e]\{q_e\} = \{F_e\}. \quad (14)$$

1.2. The Equation System 'Railway Vehicle Wheel–Track' for the Track

In order to more accurately determine the interaction between the rail and the wheel–rail, researchers assess the gap properties of the railway sleeper and the sleeper–roadbed.

The presented mathematical model for the system 'Railway Vehicle Wheel–Track' can be used for investigating the interaction between the wheel of rolling stock and the rail, when the wheel has or has no flat.

For assessing the impact of the railroad bed on the system rail–wheel–bogie, the following assumptions and evaluations can be made:

- the gap of the rail and railroad bed between two sleepers *i* and *i*+1 at the midpoint of *j* (Fig. 2);
- the interaction between soil layers under adjacent rails.

The dynamic model for the system 'Railway Vehicle Wheel–Track' and its unevenness is presented in Fig. 2.

The potential energy of an elastic element and a dissipation function of damping element $e_{pad,i}$ between the rail and the *i*th sleeper are equal to:

$$E_{p,pad,i} = \frac{1}{2} k_{pad,i} \left(w_i - q_{sl,i}\right)^2 H\left(\delta_{pad,i}\right); \quad (15)$$

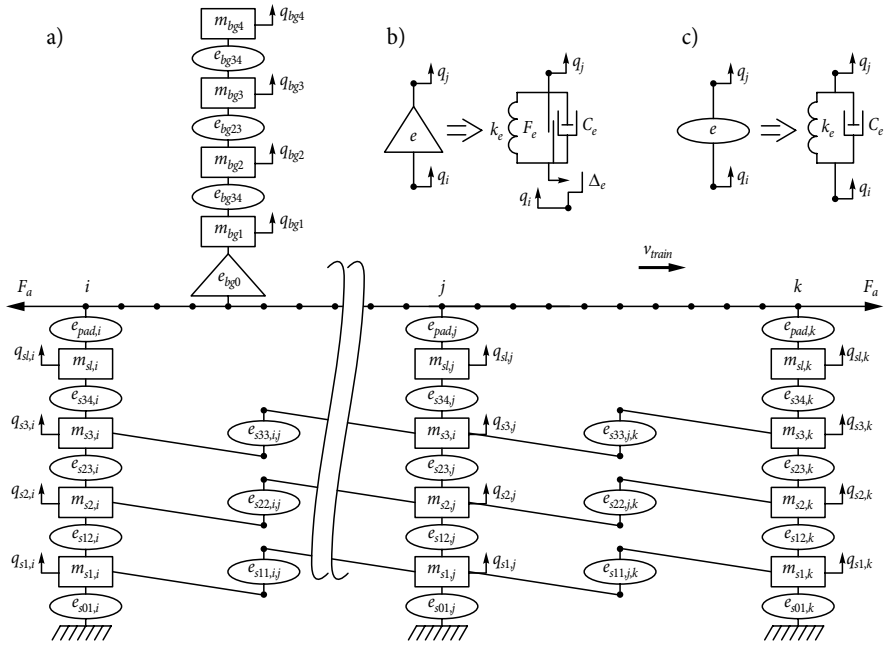

Fig. 2. Dynamic model for the system 'Railway Vehicle Wheel–Track': a – scheme; b – nonlinear elastic-damping discrete element; c – linear elastic-damping discrete element

$$\Phi_{pad,i} = \frac{1}{2} c_{pad,i} \left(\dot{w}_i - \dot{q}_{sl,i} \right)^2 H\left(\delta_{pad,i} \right); \quad (16)$$

$$\delta_{pad,i} = q_{sl,i} - w_i - \Delta_{sl,i}, \quad (17)$$

where: $H\left(\delta_{sl,i}\right)$ is the Heaviside function; $\Delta_{sl,i}$ is gaps between the rail and the *i*th sleeper; $k_{pad,i}$, $c_{pad,i}$ are the stiffness and damping coefficients of the pads; $q_{sl,i}$, $\dot{q}_{sl,i}$ are the displacement and velocity of sleepers respectively; w_i, $\dot{w}_i$ are the displacement and velocity of the rail.

The potential energy function of elastic ballast elements between *i*th and *j*th sleepers is equal to:

$$E_{p,b,i,j} = \frac{1}{2}\Big(k_{s01,i} q_{s1,i}^2 + k_{s12,i} \left(q_{s2,i} - q_{s1,i} \right)^2 + k_{s23,i} \left(q_{s3,i} - q_{s2,i} \right)^2 + k_{s34,i} \left(q_{s4,i} - q_{s3,i} \right)^2 + k_{s11,i,j} \left(q_{s1,i,} - q_{s1,j} \right)^2 + k_{s22,i,j} \left(q_{s2,i} - q_{s2,j} \right)^2 + k_{s33,i,j} \left(q_{s3,i} - q_{s3,j} \right)^2 \Big), \quad (18)$$

where: $k_{s01,i}$, $k_{s12,i}$, $k_{s23,i}$, $k_{s34,i}$, $k_{s11,i,j}$, $k_{s22,i,j}$, $k_{s33,i,j}$ are stiffness coefficients of ballast elements; $q_{s1,i}$, $q_{s2,i}$, $q_{s3,i}$ are displacements of ballast and sub ballast at the *i*th point.

A dissipation function of damping ballast elements between *i*th and *j*th sleepers is equal to:

$$\Phi_{s01,i} = \frac{1}{2}\Big(c_{s01,i} \dot{q}_{s1,i}^2 + c_{s12,i} \left(\dot{q}_{s2,i} - \dot{q}_{s1,i} \right)^2 + c_{s23,i} \left(\dot{q}_{s3,i} - \dot{q}_{s2,i} \right)^2 + c_{s34,i} \left(\dot{q}_{s4,i} - \dot{q}_{s3,i} \right)^2 + c_{s11,i,j} \left(\dot{q}_{s1,i,} - \dot{q}_{s1,j} \right)^2 + c_{s22,i,j} \left(\dot{q}_{s2,i} - \dot{q}_{s2,j} \right)^2 + c_{s33,i,j} \left(\dot{q}_{s3,i} - \dot{q}_{s3,j} \right)^2 \Big), \quad (19)$$

where: $c_{s01,i}$, $c_{s12,i}$, $c_{s23,i}$, $c_{s34,i}$, $c_{s11,i,j}$, $c_{s22,i,j}$, $c_{s33,i,j}$ are damping coefficients of ballast elements.

The system of equations for sleepers, ballast and sub-ballast blocks is established from the second order Lagrange equation:

$$\left[M_{i,j} \right] \left\{ \ddot{q}_{i,j} \right\} + \left[C_{i,j} \right] \left\{ \dot{q}_{i,j} \right\} + \left[K_{i,j} \right] \left\{ q_{i,j} \right\} = \left\{ F_{i,j} \right\}, \quad (20)$$

where: $\left[M_{i,j} \right]$, $\left[C_{i,j} \right]$, $\left[K_{i,j} \right]$, $\left\{ F_{i,j} \right\}$ are mass, damping and stiffness matrices of the ballast and sub-ballast block and a part of the rail shown in the Appendix 1; $\left\{ F_{i,j} \right\}$ is a vector of forces; $\left\{ q_{i,j} \right\}$, $\left\{ \dot{q}_{i,j} \right\}$, $\left\{ \ddot{q}_{i,j} \right\}$ are the vectors of displacement, velocity and the acceleration of ballast, the sleeper and the rail.

The vector $\left\{ q_{i,j} \right\}$ is equal to:

$$\left\{ q_{i,j} \right\}^T = \left[\left\{ q_{bi} \right\}^T \quad \left\{ q_{bj} \right\}^T \quad \left\{ q_{Rij} \right\}^T \right], \quad (21)$$

where: $\left\{ q_{bi} \right\}$, $\left\{ q_{bj} \right\}$, $\left\{ q_{Rij} \right\}$ are the vectors of the displacement of the ballast and sub ballast block and a part of the rail:

$$\left\{ q_{bi} \right\}^T = \left[q_{sl,i} \quad q_{s1,i} \quad q_{s2,i} \quad q_{s3,i} \right]; \quad (22)$$

$$\left\{ q_{bj} \right\}^T = \left[q_{sl,j} \quad q_{s1,j} \quad q_{s2,j} \quad q_{s3,j} \right]; \quad (23)$$

$$\left\{ q_{Rij} \right\}^T = \left[w_i \quad w_j \right].$$

1.3. Mathematical Model for the Wheel–Rail Contact

For analysing the interaction between the rail and the wheel, it is assumed that:

- the wheel–rail profile has potential defects (Fig. 3b);
- the unevenness of the rail surface is possible.

As regards the mathematical model for the wheel and rail, micro-unevenness, localized slip, normal and tangential forces and the moments of forces along the length of the wheel–rail contact are assessed.

Considering the above introduced mathematical model, contact length is divided into small sections where force is set in contact using Hertzian contact theory.

To determine unevenness in the contact zone of the wheel and the rail and to use Hertzian contact theory, a curvature radius of the rail must be known. Thus, rail unevenness is described using the second degree Hermit polynomials.

In order to assess rail unevenness, the rail is divided into a number of sections N_R. This number may not coincide with a finite number of rail elements. The vertical unevenness of the rail in each section is described as follows:

$$\Delta Z(\xi) = H_{01}^{(2)}(\xi) \Delta Z_i + L_{\mathrm{Re}} H_{11}^{(2)}(\xi) \frac{d\Delta Z_i}{dx} + L_{\mathrm{Re}}^2 H_{21}^{(2)}(\xi) \frac{d^2 \Delta Z_i}{dx^2} + H_{02}^{(2)}(\xi) \Delta Z_{i+1} + L_{\mathrm{Re}} H_{12}^{(2)}(\xi) \frac{d\Delta Z_{i+1}}{dx} + L_{\mathrm{Re}}^2 H_{22}^{(2)}(\xi) \frac{d^2 \Delta Z_{i+1}}{dx^2}, \quad (24)$$

where: L_{Re} is the length of the finite element of the rail; ΔZ_i, ΔZ_{i+1} are vertical unevenness at the *i*th and (*i*+1) th point; $H_{ik}^{(2)}$ is the Hermit polynomial of the second-order:

$$H_{01}^{(2)}(\xi) = 1 - 10\xi^3 + 15\xi^4 - 6\xi^5;$$

$$H_{11}^{(2)}(\xi) = -6L_{\mathrm{Re}}\xi^3 + L_{\mathrm{Re}}\xi + 8L_{\mathrm{Re}}\xi^4 - 3L_{\mathrm{Re}}\xi^5;$$

$$H_{21}^{(2)}(\xi) = \frac{1}{2}L_{\mathrm{Re}}^2\xi^2 - \frac{3}{2}L_{\mathrm{Re}}^2\xi^3 + \frac{3}{2}L_{\mathrm{Re}}^2\xi^4 - \frac{1}{2}L_{\mathrm{Re}}^2\xi^5;$$

$$H_{02}^{(2)}(\xi) = 10\xi^3 + 15\xi^4 + 6\xi^5;$$

$$H_{12}^{(2)}(\xi) = -4L_{\mathrm{Re}}\xi^3 + 7L_{\mathrm{Re}}\xi^4 - 3L_{\mathrm{Re}}\xi^5;$$

$$H_{22}^{(2)}(\xi) = \frac{1}{2}L_{\mathrm{Re}}^2\xi^3 - L_{\mathrm{Re}}^2\xi^4 + \frac{1}{2}L_{\mathrm{Re}}^2\xi^5. \quad (25)$$

The derivative of the vertical unevenness of the rail is equal to:

$$\frac{d\Delta Z(\xi)}{dx} = \frac{d\Delta Z(\xi)}{L_{Re} d\xi} =$$

$$\frac{1}{L_{Re}}\left(\frac{dH_{01}^{(2)}}{d\xi}\Delta Z_i + L_{Re}\frac{dH_{11}^{(2)}}{d\xi}\frac{d\Delta Z_i}{dx} + L_{Re}^2\frac{dH_{21}^{(2)}}{d\xi}\frac{d^2\Delta Z_i}{dx^2} + \frac{H_{02}^{(2)}}{d\xi}\Delta Z_{i+1} + L_{Re}\frac{dH_{12}^{(2)}}{d\xi}\frac{d\Delta Z_{i+1}}{dx} + L_{Re}^2\frac{dH_{22}^{(2)}}{d\xi}\frac{d^2\Delta Z_{i+1}}{dx^2}\right). \quad (26)$$

A track geometry car was used for measuring 1 kilometre of railway tracks, and the received results were recorded at the increments of 0.25 m. This stretch has been broken down into sections each of which consists of 5 points. The vertical unevenness of the rail as well as the first and second derivatives, with respect to the x coordinate, are calculated as:

$$\begin{cases} \Delta Z_R(\xi_R) = \sum_{i=1}^{5} N_i(\xi_R)\Delta Z_{R,i}; \\ \frac{d\Delta Z_R}{dx} = \frac{1}{L_{\mathrm{Re}}}\sum_{i=1}^{5}\frac{dN_i(\xi_R)}{d\xi_R}\Delta Z_{R,i}; \\ \frac{d^2\Delta Z_R}{dx^2} = \frac{1}{L_{\mathrm{Re}}^2}\sum_{i=1}^{5}\frac{d^2N_i(\xi_R)}{d\xi_R^2}\Delta Z_{R,i}, \end{cases} \quad (27)$$

where: shape functions $N_i(\xi_R)$, $i=1,...,5$ are equal to:

$$N_1(\xi_R) = \xi_R(\xi_R-1)(4\xi_R^2-1)/6;$$
$$N_2(\xi_R) = -4\xi_R(2\xi_R-1)(\xi_R^2-1)/3;$$
$$N_3(\xi_R) = (\xi_R^2-1)(4\xi_R^2-1);$$
$$N_4(\xi_R) = -4\xi_R(2\xi_R+1)(\xi_R^2-1)/3;$$
$$N_5(\xi_R) = \xi_R(\xi_R+1)(4\xi_R^2-1)/6, \quad (28)$$

where: ξ_R is local coordinate,

$$\xi_R = \left(2\frac{(x-x_i)}{x_{i+1}} - x_i\right) - 1,\ \xi_R \in [-1,1].$$

The relation between the x coordinate and local coordinate ξ_R is equal to:

$$x = x_i + \left(1+\frac{\xi_R}{2}\right)(x_{i+1}-x_i),\ x \in [x_i, x_{i+1}].$$

After using the functions $N_i(\xi_R)$, $i=1,...,5$ of the sections of the vertical unevenness of the rail, the first and second derivatives, with respect to the x coordinate, are calculated as:

$$\begin{cases} \Delta Z_R = \sum_{i=1}^{5} N_i(\xi_R)\Delta Z_{R,i}; \\ \frac{d\Delta Z_R}{dx} = \frac{1}{L_{\mathrm{Re}}}\sum_{i=1}^{5}\frac{dN_i(\xi_R)}{d\xi_R}\Delta Z_{R,i}; \\ \frac{d^2\Delta Z_R}{dx^2} = \frac{1}{L_{\mathrm{Re}}^2}\sum_{i=1}^{5}\frac{d^2N_i(\xi_R)}{d\xi_R^2}\Delta Z_{R,i}. \end{cases} \quad (29)$$

The irregularities of the rail are described as function $\Delta Z_R(x)$.

Fourier series are applied widely in engineering to solve different problems. In order to describe the geometry of the wheel flat mathematically, Fourier series are the most suitable. However, determining the number of harmonics is very important as it affects the accuracy of the obtained results.

A profile of the vehicle wheel is defined as a function of radius variable, depending on the polar angle. The radius $R_W(\theta)$ of the wheel profile is described using Fourier series:

$$R_W(\theta) = \sum_{k=1}^{NH} a_{ck}\cos(k\theta) + a_{sk}\sin(k\theta), \quad (30)$$

where: a_{ck}, a_{sk} are Fourier coefficients; NH is the number of harmonics.

A real vehicle's wheel flat and a calculation scheme for the profile of the vehicle's wheel flat are shown in Fig. 3.

The depth of the wheel flat is described as follows:

$$\Delta_F = R_{W0}\left(1-\sqrt{1-\left(\frac{L_F}{2R_{W0}}\right)^2}\right), \quad (31)$$

where: R_{W0} is a nominal wheel radius; L_F is the length of the wheel flat.

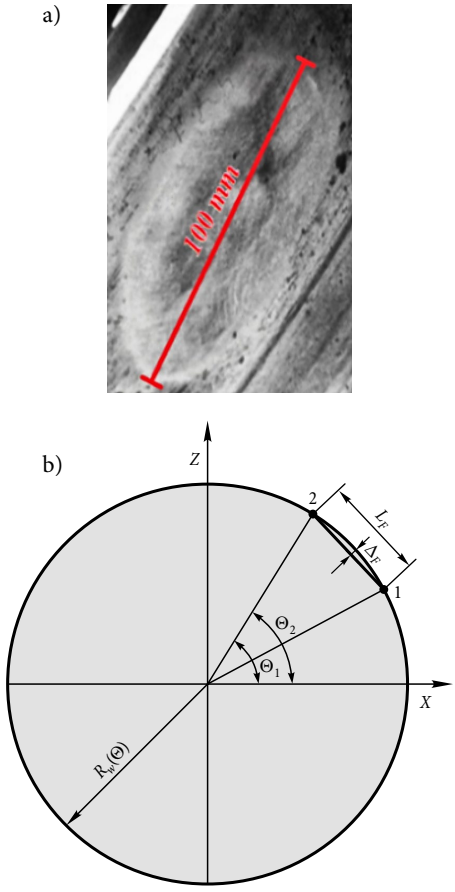

Fig. 3. Vehicle's wheel flat (a) and calculation scheme for the profile of the vehicle's wheel flat (b)

While operating, the profile of the railway wheel–rail is changing and affects wheel–rail interaction.

Wheel flats (Fig. 3a) are most commonly caused by an uneven surface, temperature differences, etc. Wheel flats of the axle occur on the tread surface. Wheel damage is usually determined visually or by template support, depending on staff qualification. To control the rolling surface, other diagnostic methods are used. For example, the application of Lenz and vibrant force sensors assist in measuring the critical values of the wheel surface with the help of comparison.

For determining wheel–rail intersection points, defining the X and Z coordinates of the wheel–rail and the rail is necessary.

Penetration rate at point k with local coordinate ξ_k of contact is:

$$\delta_k = \left[N_w\left(\xi_k\right)\right]\left\{q_e\right\} + \Delta Z_R \cos\left(\phi_k\right) - \left(q_{bg1} - \left(R_{W0} - R_W\left(\Psi_k\right)\right)\sin\left(\Psi_k\right)\right), \quad (32)$$

if $0 \le \phi_{nW} \le \pi$:

$$\begin{cases} 0 \le \Psi_k \le \phi_{nW}, & \theta_k = 2\pi - \phi_{nW} + \Psi_k; \\ \phi_{nW} < \Psi_k \le 2\pi, & \theta_k = \Psi_k - \phi_{nW}; \end{cases}$$

if $\pi < \phi_{nW} \le 2\pi$:

$$\begin{cases} 0 \le \Psi_k \le \phi_{nW}, & \theta_k = 2\pi - \phi_{nW} + \Psi_k; \\ \phi_{nW} \le \Psi_k \le 2\pi, & \theta_k = \Psi_k - \phi_{nW}; \end{cases}$$

$$\phi_{nW} = 2\pi\left(a - nW\right), \text{ when } a = \frac{\Omega t}{2\pi};$$

$$nW = \text{integer}\left(\frac{\Omega t}{2\pi}\right);$$

$$x_k = x_c - R_W\left(\theta_k\right)\cos\left(\Psi_k\right),$$

where: $R_W\left(\theta_k\right)$ is the radius of the wheel–rail profile; q_{bg1} is the vertical displacement of the wheel–rail; $\left\{q_e\right\}$ is a displacement vector for the finite element of the rail; Ψ_k is the angle (Fig. 4).

The deviation angle:

$$tg\left(\phi_k\right) = -\frac{dw_R\left(x_k\right)}{dx} = -\frac{1}{L_{\text{Re}}}\left[\frac{\partial N_w\left(\xi_k\right)}{\partial \xi}\right]\left\{q_e\right\}. \quad (33)$$

Penetration speed at the contact point is equal to:

$$\dot{\delta}_k = \left[N_w\left(\xi_k\right)\right]\left\{\dot{q}_e\right\} + \frac{V}{L_{Re}}\left[\frac{\partial N_w\left(\xi_k\right)}{\partial \xi}\right]\left\{q_e\right\} + \frac{V}{L_{Re}}\frac{d\Delta Z}{d\xi}\cos\left(\phi_k\right) - \Delta Z\dot{\phi}_k \sin\left(\phi_k\right) - \dot{q}_{bg1} - \frac{\partial R_k\left(\theta_k\right)}{\partial \theta}\Omega\sin\left(\Psi_k\right), \quad (34)$$

where: Ω is the angular velocity of the wheel set, $\Omega = V/R_{W0}$;

$$\dot{\phi}_k = -\cos^2\left(\phi_k\right)\left(\frac{1}{L_{Re}}\left[\frac{\partial N_w\left(\xi_k\right)}{\partial \xi}\right]\left\{\dot{q}_e\right\} + \frac{V}{L_{\text{Re}}^2}\left[\frac{\partial^2 N_w\left(\xi_k\right)}{\partial \xi^2}\right]\left\{q_e\right\}\right) \quad (35)$$

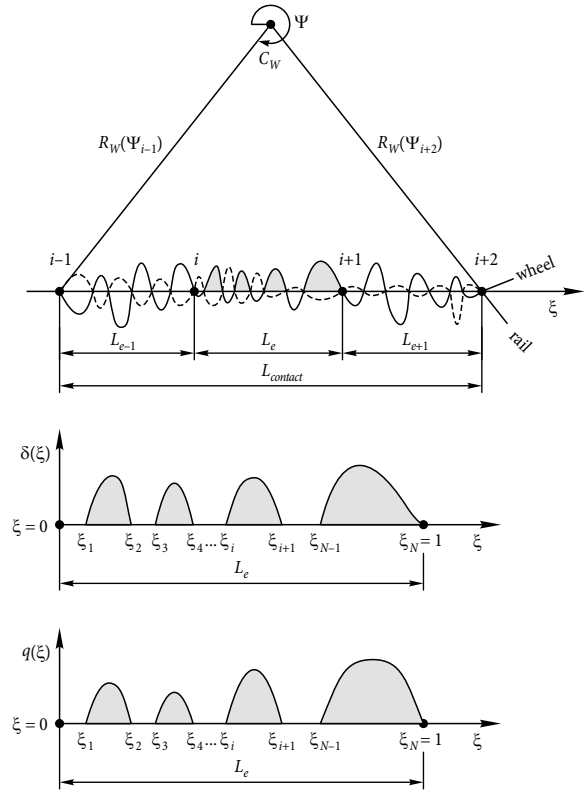

Fig. 4. The contact of the wheel and rail: a – changes in penetration in the contact area; b – chart of speed and forces operating at point k of the vehicle's wheel and rail

Force $F_{contact}\left(x\right)$ appearing at the contact point is determined using Hertzian contact theory. In addition, the hysteresis of contact forces is evaluated:

$$F_{contact}\left(x\right) = k_{RW}\left(x\right)\delta\left(x\right)^n D\left(\dot{\delta}\left(x\right)\right)H\left(\delta\left(x\right)\right), \quad (36)$$

where:

$$k_{RW}\left(x\right) = \frac{4}{3}E_{ekv}\sqrt{R\left(x\right)}; \quad (37)$$

$$\frac{1}{E_{ekv}} = \frac{1-\nu_R^2}{E_R} + \frac{1-\nu_W^2}{E_W}; \quad (38)$$

$$R\left(x\right) = \frac{R_R\left(x\right)R_W}{R_R\left(x\right) + R_W}; \quad (39)$$

$$D\left(\dot{\delta}\right) = 1 + \frac{3}{4}\left(1-e^2\right)\frac{\dot{\delta}}{\dot{\delta}_{\max}}, \quad (40)$$

where: k_{RW} is contact stiffness, e is speed restitution coefficient; E_R, E_W are the modulus of elasticity of the rail and wheel; ν_R, ν_W are Poisson's coefficients of the rail and wheel; R_W estimated by (Eq. 30); rail radius R_R is equal to:

$$R_R\left(x_k\right) = \frac{\left(1 + \left(\frac{d\Delta Z\left(x_k\right)}{dx}\right)^2 + \frac{dw}{dx}\right)^{\frac{3}{2}}}{\left(\frac{d^2\Delta Z\left(x_k\right)}{dx^2}\right)} + \frac{d^2w}{dx^2}, \quad (41)$$

where the derivatives of the vertical unevenness of the rail equal:

$$\frac{d\Delta Z(x_k)}{dx}=\frac{1}{L_{\mathrm{Re}}}\sum_{i=0}^{2}\sum_{j=1}^{2}\left(\frac{dH_{ij}^{(2)}(\xi_k)}{d\xi}\frac{d^i\Delta Z_j}{dx^i}\right); \quad (42)$$

$$\frac{d^2\Delta Z(x_k)}{dx^2}=\frac{1}{L_{\mathrm{Re}}^2}\sum_{i=0}^{2}\sum_{j=1}^{2}\left(\frac{d^2H_{ij}^{(2)}(\xi_k)}{d\xi^2}\frac{d^i\Delta Z_j}{dx^i}\right). \quad (43)$$

The alteration of penetration in the contact of the wheel and rail evaluating the unevenness of the wheel and rail, forces operating in the *k*th point of the contact of the wheel and rail and velocity are shown in Fig. 4.

Load distribution in the interval $x\in\left[x_1...x_{NP}\right]$ in the contact area is equal to:

$$q(x)=\frac{dF_{contact}(x)}{dx}=\frac{dF_{contact}(x)}{dk_{RW}}\frac{dk_{RW}(x)}{dx}+$$
$$\frac{dF_{contact}(x)}{dR}\frac{dR(x)}{dx}+\frac{dF_{contact}(x)}{d\delta}\frac{d\delta(x)}{dx}; \quad (44)$$

$$\frac{dk_{RW}(x)}{dx}=\frac{dk_{RW}}{dR}\left(\frac{dR}{dR_R}\frac{dR_R}{dx}\right); \quad (45)$$

$$\frac{dR}{dR_R}=\frac{R_W^2}{\left(R_R+R_W\right)^2}; \quad (46)$$

$$\frac{dk_{RW}}{dR}=\frac{2}{3}E_{ekv}\frac{1}{\sqrt{R(x)}}. \quad (47)$$

By using expressions (32–47), load distribution in the local coordinate system is equal to:

$$q(\xi)=\frac{dF_{contact}(\xi)}{L_e d\xi}=\frac{dF_{contact}(\xi)}{dk_{RW}}\frac{dk_{RW}(\xi)}{L_e d\xi}+$$
$$\frac{dF_{contact}(\xi)}{dR}\frac{dR(\xi)}{L_e d\xi}+\frac{dF_{contact}(\xi)}{d\delta}\frac{d\delta(\xi)}{L_e d\xi}. \quad (48)$$

The load vector of the *e*th finite element of the rail in contact length (Fig. 5) is equal to:

$$\left\{F_e\right\}=\sum_{i=1}^{ne}\int_{\xi_i}^{\xi_{i+1}}\left[N_w(\xi)\right]^T q(\xi)L_e d\xi, \quad (49)$$

where: *ne* is the number of contact intervals in the finite element of the rail, when penetration is positive ($\delta\geq 0$) in all contact interval $\xi\in\left[\xi_i,\xi_{i+1}\right]$.

Vertical force affects the mass of the wheel in the contact interval and is equal to:

$$F_{BW}=\sum_{e}\sum_{i=1}^{ne}\int_{\xi_i}^{\xi_{i+1}}q_e(\xi)L_e d\xi. \quad (50)$$

The coordinate $x_{cont,aver,q}\in\left[x_1,...,x_{NP}\right]$ of load distribution operating in the contact interval is equal to:

$$x_{cont,aver,q}=\frac{\int_{x_1}^{x_{NP}}xq(x)dx}{\int_{x_1}^{x_{NP}}q(x)dx}, \quad (51)$$

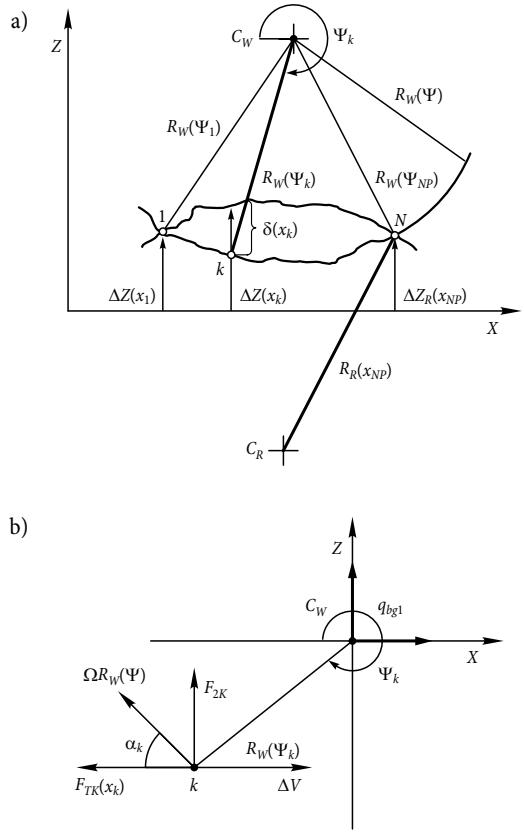

Fig. 5. Wheel and rail geometric parameters for the contact area

where: *NP* is the number of points in the contact interval.

The coordinate of resultant penetration at the finite element of the rail in contact zone $x_{aver,\delta}$ is equal to:

$$x_{aver,\delta}=\frac{\int_{x_1}^{x_{NP}}x\delta(x)dx}{\int_{x_1}^{x_{NP}}\delta(x)dx}, \quad (52)$$

where: x_1 and x_{NP} are rail coordinates *x*.

Contact load and displacement vectors of the finite elements of the rail and wheel as well as force acting in the contact are equal to:

$$\left\{F_{R,BW}\right\}^T=\left\{\left\{F_{\mathrm{Re}}\right\}^T,F_{BW}\right\}; \quad (53)$$

$$\left\{q_{R,BW}\right\}^T=\left[\left\{q_{\mathrm{Re}}\right\}^T,q_{bg1}\right]. \quad (54)$$

Vector $\left\{F_{R,BW}\right\}$ is expanded in the surroundings of point $\left\{q_{R,BW,k}\right\}$ using *Taylor series* and is equal to:

$$\left\{F_{R,BW,k+1}\right\}=\left\{F_{R,BW,k}\right\}+\left[K_{T,R,BW,k}\right]\left\{\Delta q_{R,BW,k}\right\}, \quad (55)$$

where: $\left[K_{T,RBC,k}\right]$ is the Jacobi matrix,

$$\left[K_{T,RBC,k}\right]=\begin{bmatrix}\left[K_{T,R,R,k}\right] & \left[K_{T,R,BW,k}\right]\\ \left[K_{T,BW,R,k}\right] & \left[K_{T,BW,BW,k}\right]\end{bmatrix}=$$

$$\begin{bmatrix}\left[\frac{\partial\{F_R\}}{\partial\{q_{\mathrm{Re}}\}}\right] & \left[\frac{\partial\{F_R\}}{\partial q_{bq1}}\right]\\ \left[\frac{\partial\{F_{BW}\}}{\partial\{q_{\mathrm{Re}}\}}\right] & \left[\frac{\partial\{F_{BW}\}}{\partial q_{bq1}}\right]\end{bmatrix}, \quad (56)$$

where: $\{\Delta q_{RB,k}\}$ is an increment of displacement vector $\{q_{R,BW,k}\}$.

The system of nonlinear equations for the finite elements of rails in contact with wheel mass is equal to:

$$\left[M_{R,BW}\right]\{\ddot{q}_{R,BW}\}+\left[C_{R,BW}\right]\{\dot{q}_{R,BW}\}+\left[K_{R,BW}\right]\{q_{R,BW}\}-$$

$$\left[K_{T,R,BW,k}\right]\{\Delta q_{R,BW,k}\}=\{F_{R,BW}(t)\}+\{F_{R,BW,k}\}, \quad (57)$$

where: $\{F_{R,BW}(t)\}$ is force varying in time; $\{F_{R,BW,k}\}$ is nonlinear force dependant on point k; $\left[M_{R,BW}\right]$, $\left[C_{R,BW}\right]$, $\left[K_{R,BW}\right]$ are mass, damping and stiffness matrices respectively,

$$\left[M_{R,BW}\right]=\begin{bmatrix}\left[M_{Re}\right] & [0]\\ [0] & \left[m_{bg1}\right]\end{bmatrix}; \quad (58)$$

$$\left[C_{R,BW}\right]=\begin{bmatrix}\left[C_{Re}\right] & [0]\\ [0] & [0]\end{bmatrix}; \quad (59)$$

$$\left[K_{R,BW}\right]=\begin{bmatrix}\left[K_{Re}\right] & [0]\\ [0] & [0]\end{bmatrix}. \quad (60)$$

Knowing the contact points of wheel–rail length (Fig. 5), at each of these places, a longitudinal relative wheel slip can be determined in the following way:

$$\varepsilon(\xi)=\frac{\Delta V(\xi)}{V}, \quad (61)$$

where:

$$\Delta V=V-\Omega R_W(\Psi_k)\cos(\Psi_k)-\dot{u}_k; \quad (62)$$

$$\dot{u}_k=\left(\frac{h_k+\Delta Z(\xi_k)}{L_e}\right)\left[\frac{dN_w(\xi_k)}{d\xi}\right]\{\dot{q}_e\}+$$

$$V\frac{\left(h_k+\Delta Z(\xi_k)\right)}{L_e^2}\left[\frac{d^2N_w(\xi_k)}{d\xi^2}\right]\{q_e\}, \quad (63)$$

where: h_k is the distance from the geometric centre to the surface of the rail head.

Friction force in the contact interval is equal:

$$F_{TK}=\sum_e\sum_{i=1}^{ne}F_{BW,e,i}\mu(\varepsilon_{e,i}), \quad (64)$$

where: $\varepsilon_{e,i}$ is a wheel slip in the ith point of the eth finite element of the rail, $\varepsilon_{e,i}=\frac{\Delta V(\xi_i)}{V}$; $\mu(\varepsilon_{e,i})$ is the friction coefficient between the rail and wheel.

When using expressions (49) and (63), resultant resistance force and torque about the Y axis of the wheel depend on friction and normal forces in the contact and are equal to:

$$F_{X,Friction}=-\sum_e\sum_{i=1}^{ne}F_{BW,e,i}\mu(\varepsilon_{e,i})\cos(\alpha_{e,i}); \quad (65)$$

$$M_Y=\sum_e\sum_{i=1}^{ne}F_{BW,e,i}\mu(\varepsilon_{e,i})R_W(\Psi_{e,i})+$$

$$F_{BW,e,i}R_W(\Psi_{e,i})\sin(\alpha_{e,i}); \quad (66)$$

where: e is the number of the finite element of the rail; i is the point of the wheel–rail contact; $\alpha_{e,i}$ is the angle between the vertical axis of the wheel and radius.

1.4. System for Equations for a Railway Vehicle

1/8 of the vehicle body with cargo mass, 1/4 of bogie mass and 1/2 of wheel set mass have been assessed in the mathematical model for the railway vehicle.

As for the revised method of contact force, the wheel is divided into two masses, where mass m_{bg1} is in direct contact with the rail while mass m_{bg2} is the main mass of the wheel set. The use of the additional mass m_{bg1} of the wheel enables a more accurate assessment of forces acting in contact and the calculation of kinetic parameters for individual parts of the wheel.

A system for the nonlinear equation for railway vehicle movement out of contact is equal to:

$$\left[M_{bg}\right]\{\ddot{q}_{bg}\}+\left[C_{bg}\right]\{\dot{q}_{bg}\}+\left[K_{bg}\right]\{q_{bg}\}=$$

$$\{F_{BW}(q_{bg}\ q_{\mathrm{Re}}\ \dot{q}_{bg}\ \dot{q}_{\mathrm{Re}})\}+\{F_{bg}(t)\}, \quad (67)$$

where: $\{q_{bg}\}^T=\left[q_{bg1}\ q_{bg2}\ q_{bg3}\ q_{bg4}\right]$; q_{bgi} is the displacement of the mass of the ith vehicle; $\left[M_{bg}\right]$, $\left[C_{bg}\right]$, $\left[K_{bg}\right]$, $\{F_{BW}(q_{bg}\ q_{Re}\ \dot{q}_{bg}\ \dot{q}_{Re})\}$, $\{F_{bg}(t)\}$ are mass, damping and stiffness matrices, nonlinear load and weight force vectors respectively. The introduced matrices and vectors are shown in Appendix 2.

The nonlinear load vector is equal to:

$$\{F_{BW}(q_{bg}\ q_{\mathrm{Re}}\ \dot{q}_{bg}\ \dot{q}_{\mathrm{Re}})\}=\left[F_{contact}(q_{bg}\ q_{Re}\ \dot{q}_{bg}\ \dot{q}_{Re})\right].$$

The total nonlinear equation system for the whole movement system is equal to:

$$\left[M\right]\{\ddot{q}\}+\left[C\right]\{\dot{q}\}+\left[K\right]\{q\}+\{F_{NL}(q,\dot{q})\}=\{F(t)\}, \quad (68)$$

where: $\left[M\right]$, $\left[C\right]$, $\left[K\right]$, $\{F_{NL}(q,\dot{q})\}$, $\{F(t)\}$ are mass, damping and stiffness matrices and nonlinear load and external force vectors respectively; $\{q\}^T=\left[\{q_R\}^T,\{q_B\}^T,\{q_{bg}\}^T\right]$ is the total displacement vector; $\{q_R\}$ is a displacement vector of the rail; $\{q_S\}$ is a displacement vector of ballast; $\{q_{bg}\}$ is a displacement vector of the vehicle.

The nonlinear total system of equations for motion is solved applying Newmark (1947) and Newton–

Raphson method. The accuracy of the solution to the nonlinear problem is increased by combining the above methods.

Non-linear force $\{F_{NL}(q,\dot{q})\}$ is extracted in the Taylor series at the surroundings of point $\{q_k\}$:

$$\{F_{NL}(q,\dot{q})\}=\{F_{NL,k}\}+[K_{T,k}]\{\Delta q_k\}+[C_{T,k}]\{\Delta\dot{q}_k\}, \tag{69}$$

where:

$$[K_{T,k}]=\left[\frac{\partial\{F_{NL}(q_k,\dot{q}_k)\}}{\partial\{q\}}\right];$$

$$[C_{T,k}]=\left[\frac{\partial\{F_{NL}(q_k,\dot{q}_k)\}}{\partial\{\dot{q}\}}\right].$$

Then, the total system of equations (33), at the moment of time $t + \Delta t$, is equal to:

$$[M]\{\ddot{q}_{t+\Delta t}\}+[C]\{\dot{q}_{t+\Delta t}\}+[K]\{q_{t+\Delta t}\}+$$
$$[C_T]\{\Delta\dot{q}_{t+\Delta t,k}\}+[K_T]\{\Delta q_{t+\Delta t,k}\}=$$
$$-\{F_{NL}(q_{t+\Delta t},\dot{q}_{t+\Delta t})\}+\{F(t)\}. \tag{70}$$

When applying Newmark (1947) and Newton–Raphson methods, the total system for linear algebraic equations is solved in each of kth iterations:

$$[A_{t+\Delta t,k}]\{\Delta q_k\}=-\{P_{t+\Delta t,k}\}, \tag{71}$$

where:

$$[A_{t+\Delta t,k}]=\left(\frac{1}{\beta\Delta t^2}[M]+\right.$$
$$\left.\frac{\gamma}{\beta\Delta t}([C]+[C_{T,k}])+([K]+[K_{T,k}])\right);$$
$$\{P_{t+\Delta t,k}\}=[M]\{\ddot{q}_{t+\Delta t,k}\}+[C]\{\dot{q}_{t+\Delta t,k}\}+$$
$$[K]\{q_{t+\Delta t,k}\}+\{F_{NL,k}\}-\{F(t+\Delta t)\},$$

where: β, γ are the Newmark's coefficients: $\gamma=1/2$, $\beta=1/4$; Δt is integration time step; t is time.

At the initial moment of time $t = 0$, displacement vector $\{q_{t+\Delta t,k}\}$ is determined from the equation system:

$$\begin{cases}([K]+[K_{T,k}])\{\Delta q_{t+\Delta t,k}\}=-\{P(q_{t+\Delta t,k})\};\\ \{q_{t+\Delta t,k+1}\}=\{q_{t+\Delta t,k}\}+\{\Delta q_{t+\Delta t,k}\}.\end{cases} \tag{72}$$

2. Results of Mathematical Modelling

2.1. Parameters for the System 'Railway Vehicle Wheel–Track'

In order to compile the mathematical model for the system 'Railway Vehicle Wheel–Track', data on the four-axle freight vehicle 12–9780 were used. It is assumed that the vehicle moves at a speed of 100 km per hour. The fat of the vehicle wheel is L_F = 100 mm. A static load on the rail is 100 kN. It has been calculated that the rail has no unevenness.

Table 1. Data calculation. Track and vehicle system

Definition	Notation
Static load	$F_x = 100$ kN
The second moment of the area of the rail about Y axis	$J_{yR} = 3.54\cdot10^{-5}$ m^4
Cross-sectional area of the rail	$A_R = 82.65\cdot10^{-4}$ m^2
Poisson's coefficient of the rail	$\nu_R = 0.30$
Elastic modulus of the rail	$E_R = 206$ GPa
Rail density	$\rho_R = 7850$ kg/m^3
Rail mass per meter	$m_R = 65$ kg/m
Pad damping coefficient	$C_{pad} = 45$ kNs/m
Pad stiffness	$k_{pad} = 140$ MN/m
Sleeper spacing	$L_p = 0.5435$ m
Sleeper mass	$m_{sl} = 265$ kg
Damping coefficient of ballast	$C_{s11,i,j} = 10$ kNs/m $C_{s22,i,j} = 13$ kNs/m $C_{s33,i,j} = 15$ kNs/m $C_{s01} = 90$ kNs/m $C_{s12} = 70$ kNs/m $C_{s23} = 60$ kNs/m $C_{s34} = 50$ kNs/m
Stiffness coefficient of ballast	$k_{s11,i,j} = 15$ MN/m $k_{s22,i,j} = 16$ MN/m $k_{s33,i,j} = 17$ MN/m $k_{s01} = 180$ MN/m $k_{s12} = 170$ MN/m $k_{s23} = 160$ MN/m $k_{s34} = 150$ MN/m
Mass of ballast	$m_{s1} = 500$ kg $m_{s2} = 300$ kg $m_{s3} = 200$ kg
1/8 of the car body mass 1/4 bogie mass 1/2 of the wheel set mass Mass of the wheel in contact	$m_{bg4} = 8743$ kg $m_{bg3} = 700$ kg $m_{bg2} = 640$ kg $m_{bg1} = 110$ kg
Car body stiffness Bogie stiffness Wheel set stiffness	$k_{bg34} = 2{,}55$ MN/m $k_{bg23} = 6.5$ MN/m $k_{bg12} = 56$ MN/m
Damping coefficient of the car body Damping coefficient of the bogie Damping coefficient of the wheel set Damping coefficient of mass in contact	$C_{bg4} = 10$ kNs/m $C_{bg3} = 100$ kNs/m $C_{bg2} = 50$ kNs/m $C_{bg1} = 44.2$ kNs/m
Wheel radius Elastic modulus of the wheel Poisson's coefficient of the wheel Exponent Maximal penetration velocity Restitution coefficient Friction coefficient	$R_W = 0.495$ m $E_W = 210$ GPa $\nu_W = 0.30$ $\eta = 3/2$ $\delta_{max} = 10$ m/s $e = 0.65$ $\mu = 0.3$

The distance between sleepers is 0.5435 m, the number of sleepers is equal to 41 and is divided into 10 beam finite elements.

The number points in the contact interval are equal to NP = 1001. The total time of vehicle motion is 0.560 s,

integration time step is $\Delta t = 10^{-6}$ s. The total number of unknowns is 970.

The parameters for the developed system are presented in Table 1.

2.2. Research and Analysis of the Dynamic Process of the System 'Railway Vehicle Wheel–Track'

The carried out research is aimed at determining the forces operating under the interaction between the wheel flat and the rail and at investigating the impact of forces on the dynamics of the rail. The wheel loses contact with the railway track due to the rail, sleepers, high stiffness of the rail bed and low damping, dynamic properties of a vehicle, a high speed of the vehicle and a significant wheel flat.

The initial centre of the vehicle wheel coincides with the geometrical centre of the sleeper. The initial position of the flat is in the middle of the top of the wheel (Fig. 6).

The initial displacements of the rail under a static load on the rail of 100 kN are shown in Fig. 7. The initial position of the wheel ($t = 0$) is on the eleventh sleeper ($x = 5.47$ m).

The geometrical parameters of the wheel flat include $R_{W0} = 0.495$ m and $L_F = 100$ mm. A profile of the wheel flat of the railway vehicle is described using a four hundred and one harmonics ($NH = 401$) (Eq. 30) (Figs 8–9).

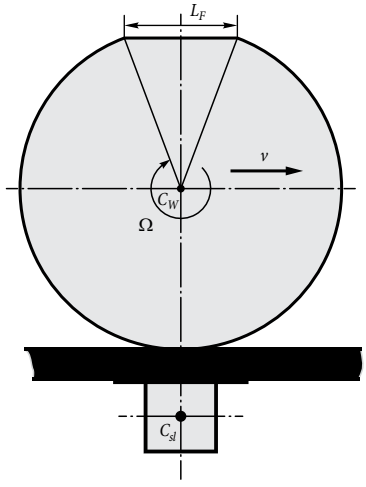

Fig. 6. The initial position of the wheel

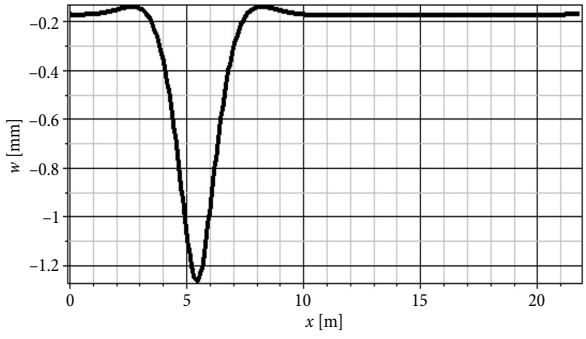

Fig. 7. The initial displacements of the rail under a static load equal to 100 kN

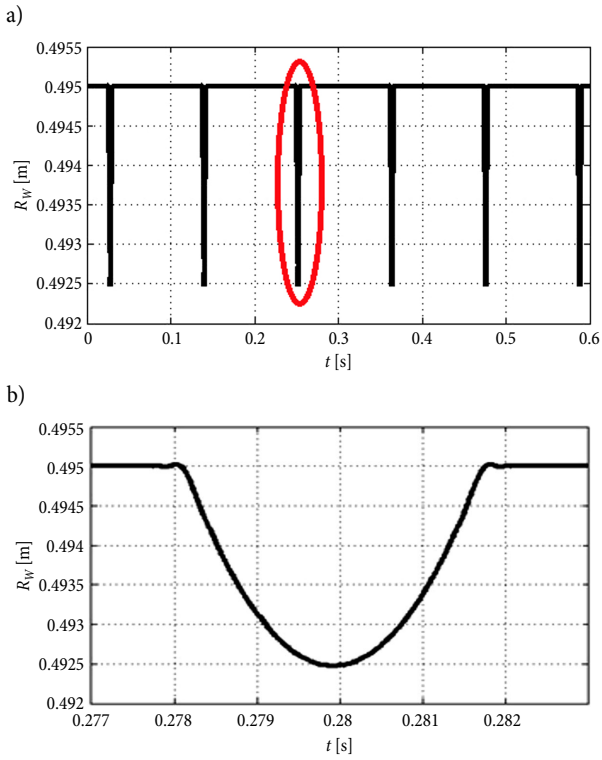

Fig. 8. Changes in the effective rolling radius of the rotating wheel flat: a – defined under the time from 0 to 0.6 s; b – defined under the time from 0.277 to 0.283 s

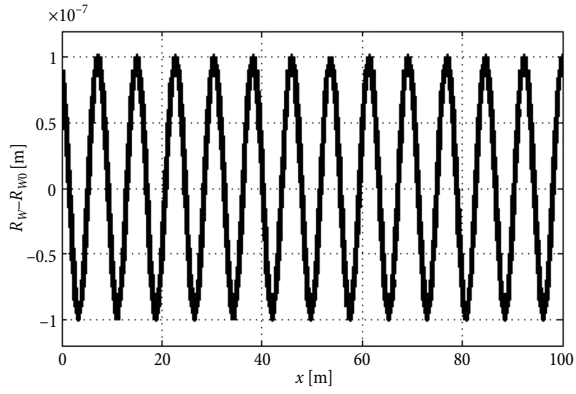

Fig. 9. A deviation of wheel radius from the nominal radius under the flat length of $L_F = 100$ mm

A deviation of wheel radius from the nominal radius when the length of the flat is equal to $L_F = 100$ mm is shown in Fig. 9.

Changes in vertical force F_Z operating upon the wheel over time are shown in Fig. 10. Due to the wheel flat ($L_F = 100$ mm, $\Delta_F = 2.53$ mm), load (100 kN) and vehicle velocity is 100 km/h, in time gaps from 0.388 to 0.398 s, wheel loses its contact with the rail (Fig. 10b).

In order to determine whether the vehicle wheel has flats, forces operating on sleepers when the wheel passes a certain section of railway rails have to be identified.

Forces operating from the rail (through the pad) are shown in Fig. 11.

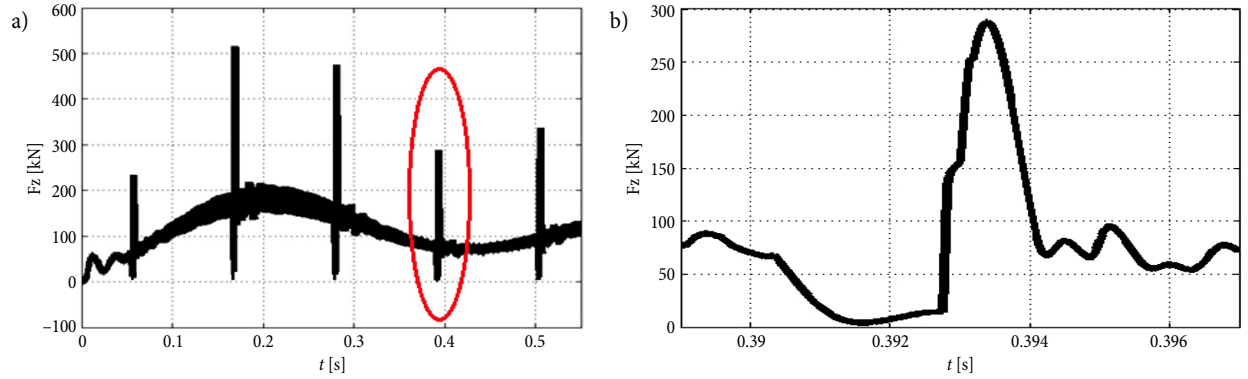

Fig. 10. Changes in vertical force F_Z operating upon the wheel over time: a – to 0.55s; b – from 0.388 to 0.398 s

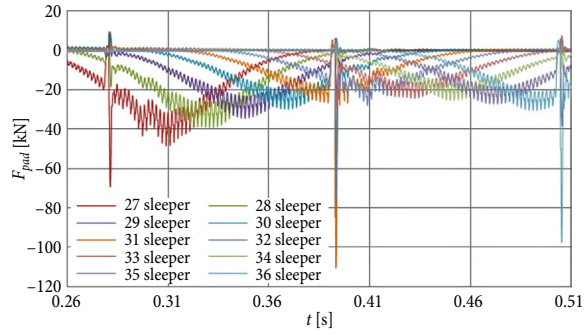

Fig. 11. Forces operating on sleepers from the rail (through the pad)

Forces on operating sleepers from the rail (through pad) are shown in Table 2.

Fig. 11 and Table 2 show that an impact on the rail occurs between the 31 and the 32, id est., at a distance of 0.2065 m from the centre of the 31th sleeper.

Impact force on the rail affects four sleepers, and both sides obtain the mostly affected sleeper (31 sleeper).

When the wheel with no flat passes through the rail, the load (from 31 sleeper) to sleepers distributes almost evenly to both sides. However, when the wheel has a flat, 31 and 32 sleepers are mostly loaded, and the load to other adjacent sleepers is almost evenly distributed to both sides.

The acceleration of the wheel is one of the most characteristic parameters evaluating a dynamic load on the rail and vehicle.

Changes of accelerations of masses m_{bg2}, m_{bg3}, m_{bg4} due to vehicle wheel flat are shown in Fig. 12

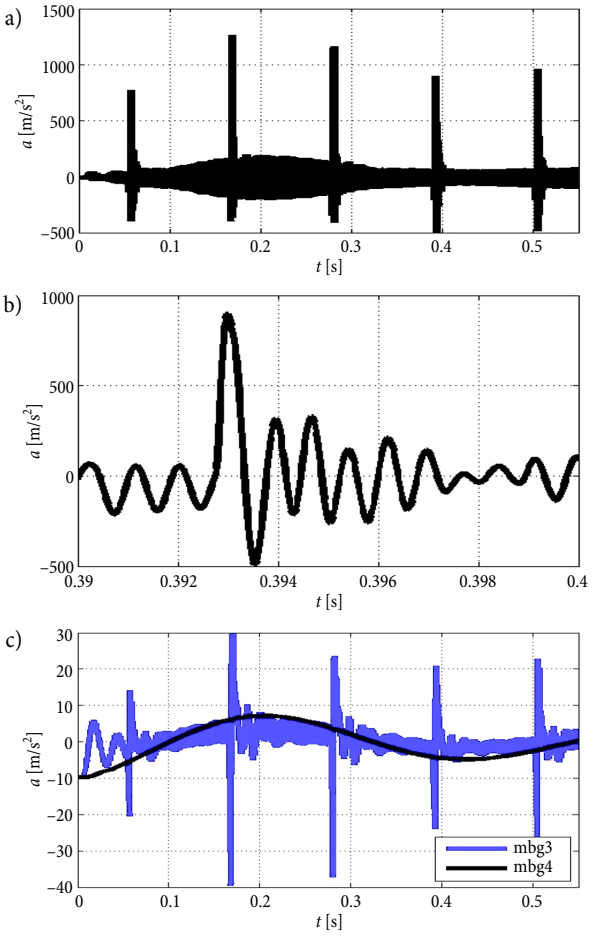

Fig. 12. Acceleration changes over time: a – m_{bg2}; b – m_{bg2} at time 0.39–0.40 s; c – m_{bg3} and m_{bg4}

Table 2. Peak forces operating on sleepers from the rail (through pad) and their percentages when the wheel has or has no flat

Measurement units	27	28	29	30	31	32	33	34	35	36
	Number of sleepers									
Value of force when the wheel has no flat at the time of 0.3931 s										
[kN]	0.9	–0.7	–6	–15	–26	–21	–9	–2	0.4	0.7
[%]	–3	3	21	58	100	81	34	8	–1	–3
Value of force when the wheel has a flat at the time of 0.39504 s										
[kN]	3.1	5.0	–7	–55	–111	–68	–14	4	3.5	0.5
[%]	–3	–4	7	50	100	62	12	–4	–3	0

The maximum value of the acceleration of mass m_{bg2} are equal to 1200 m/s^2 and the acceleration of the vehicle body mass m_{bg4} – 6.7 m/s^2. However, (Fig. 12a), the pending system shows that, up to the time of 0.30 s, a transitional process can be observed; therefore, the maximum acceleration of the wheel is equal to 900 m/s^2 when time t = 0.5 s and the acceleration of the mass of the car body m_{bg4} is 0.7 m/s^2.

Sudden changes in vehicle accelerations are seen in the acceleration curve (Fig. 12a) (at time: 0.06, 0.17, 0.28, 0.39, 0.50 s) when wheel impact occurs on the rail.

Acceleration spectra of the wheel set and vertical forces occurring in contact between the wheel and the rail (Fig. 13) are determined using discrete Fourier transform.

The maximum amplitude of vertical wheel force (40 kN) can be observed at frequency f = 503 Hz that is approximately obtained examining the system: body–springs, i.e:

$$f = \frac{1}{(2\pi)}\sqrt{\frac{k_{RW}}{\sum m_{bgi}}} = \frac{1}{(2\pi)}\sqrt{\frac{10^{11}}{10^4}} = 503 \text{ Hz}.$$

The maximum value of the acceleration amplitude is achieved at 1006 Hz, i.e., the frequency of acceleration is equal to 2f.

The history of time for the displacements of vehicle mass in the dynamic system 'Railway Vehicle Wheel–Track' is shown in Fig. 14.

The alterations of displacements, under an impact between the wheel flat and the rail (Fig. 14), demonstrate that the vertical displacements of the wheel set are altered most, but the displacements of the bogie and body vary to a small extent (Fig. 14a). The loss of contact is observed by comparing the displacements of the wheel flat (Fig. 14b), after impact forces (0.06, 0.17, 0.28, 0.39, 0.50 s) occur in the contact area due to the wheel flat.

Conclusions

The article has proposed the revised contact force method, which, unlike the model of two or more interacting points, is based on the split of the contact zone to a set number of intervals. It allows determining forces and other contact characteristics occurring in the contact zone of the wheel and rail at any moment of time.

Describing the unevenness of the system 'Railway Vehicle Wheel–Track' possibly appearing in contact between the wheel flat and the rail, short-term gaps between the wheel and rail, and possible gaps between the rail and sleepers have been evaluated.

The system 'Railway Vehicle Wheel–Track' has been examined under a wheel flat of 100 mm, a velocity of 100 km/h and a static load of 100kN. The computational model consists of the vehicle and the track divided into finite elements. It is assumed, that the rail has no irregularities in calculations.

The obtained results have shown that the wheel loses its contact with the rail when a flat (L_F = 100 mm and Δ_F = 2.53 mm) appears in the wheel rail contact zone under a velocity of v = 100 km/h.

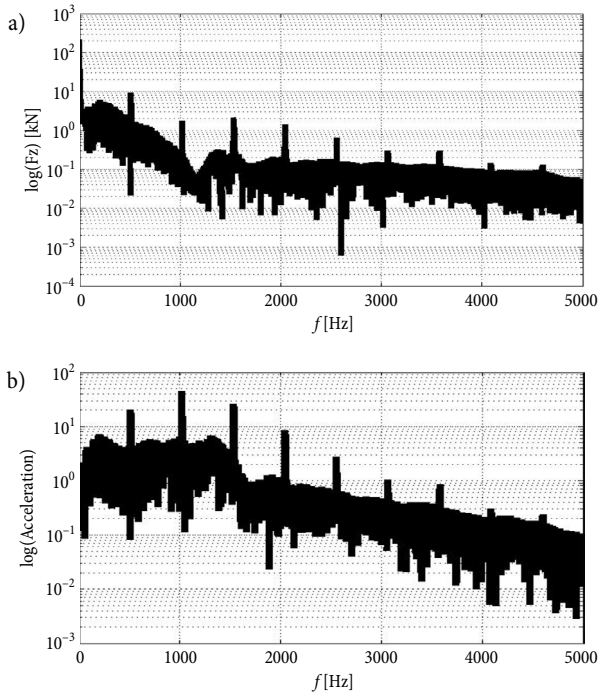

Fig. 13. Parameters occurring in contact between the vehicle's wheel flat and the rail: a – amplitude of the vertical force; b – amplitude of wheel set acceleration

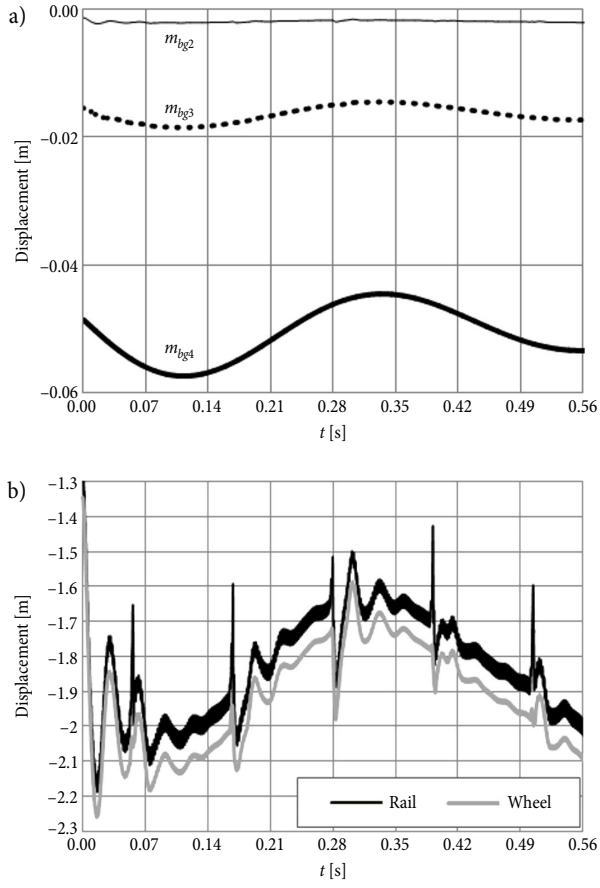

Fig. 14. The history of time for displacements: a – wheel flat (L = 100 mm); b – wheel and rail

Comparative research has shown that the vertical contact force of the wheel occurring from the wheel to the rail is distributed into four sleepers to both sides.

The study has shown that, by using the revised contact force method, the problems of wheel and rail wear can be examined, and the forces occurring in contact between the wheel flat and the rail can be identified. Its size and the points where wheel flats occur can be determined more accurately.

Further studies suggest examining the forces occurring within wheel bearings, in contact between the wheel flat and the rail, using the revised contact force method.

Acknowledgements

This work has been supported by the European Social Fund within the project 'Development and application of innovative research methods and solutions for traffic structures, vehicles and their flows', project code VP1-3.1-ŠMM-08-K-01-020.

References

Ahmetzyanov, M. H. 2003. O mehanizme razvitiya kontaktno-ustalostnyh povrezhdenij v rel'sah, *Vestnik Nauchno-Issledovatel'skogo Instituta Zheleznodorozhnogo Transporta* (2): 41–45. (in Russian).

Aursudkij, B. 2007. *A Laboratory Study of Railway Ballast Behaviour Under Traffic Loading and Tamping Maintenance*: Thesis submitted to the University of Nottingham for the degree of Doctor of Philosophy. 234 p. Available from Internet: http://eprints.nottingham.ac.uk/10321

Barke, D. W.; Chiu, W. K. 2005. A review of the effects of out-of-round wheels on track and vehicle components, *Proceedings of the Institution of Mechanical Engineers, Part F: Journal of Rail and Rapid Transit* 219(3): 151–175. http://dx.doi.org/10.1243/095440905X8853

Bezin, Y.; Iwnicki, S. D.; Cavalletti, M.; De Vries, E.; Shahzad, F.; Evans, G. 2009. An investigation of sleeper voids using a flexible track model integrated with railway multi-body dynamics, *Proceedings of the Institution of Mechanical Engineers, Part F: Journal of Rail and Rapid Transit* 223(6): 597–607. http://dx.doi.org/10.1243/09544097JRRT276

Bian, J.; Gu, Y.; Murray, M. H. 2013. A dynamic wheel–rail impact analysis of railway track under wheel flat by finite element analysis, *Vehicle System Dynamics* 51(6): 784–797. http://dx.doi.org/10.1080/00423114.2013.774031

Bogacz, R.; Krzyżynski, T.; Popp, K. 1993. On vertical and lateral dynamics of periodic guideways for maglev vehicle, in R. Bogacz, K. Popp (Eds.). *Dynamical Problems in Mechanical Systems: Proceedings of the 3rd Polish-German Workshop*, 26–31 July 1993, Polish Academy of Sciences, Warszawa, Poland, 219–233.

Donzella, G.; Mazzù, A.; Petrogalli, C. 2009. Competition between wear and rolling contact fatigue at the wheel–rail interface: some experimental evidence on rail steel, *Proceedings of the Institution of Mechanical Engineers, Part F: Journal of Rail and Rapid Transit* 223(1): 31–44. http://dx.doi.org/10.1243/09544097JRRT161

Ferrara, R.; Leonardi, G.; Jourdan, F. 2012. Numerical modelling of train induced vibrations, *Procedia – Social and Behavioral Sciences* 53: 155–165. http://dx.doi.org/10.1016/j.sbspro.2012.09.869

Herron, D.; Jones, C.; Thompson, D.; Rhodes, D. 2009. Characterising the high-frequency dynamic stiffness of railway ballast, in M. Pawelczyk, D. Bismor (Eds.). *Proceedings of the 16th International Congress on Sound and Vibration: Recent Developments in Acoustics, Noise and Vibration (ICSV16)*, 5–9 July 2009, Kraków, Poland, 1–8. Available from Internet: http://resource.isvr.soton.ac.uk/staff/pubs/PubPDFs/Pub11199.pdf

Kaewunruen, S.; Remennikov, A.; Aikawa, A.; Sakai, H. 2014. Free vibrations of interspersed railway track systems in three-dimensional space, *Acoustics Australia* 42(1): 20–26.

Kalker, J. J. 1979. The computation of three-dimensional rolling contact with dry friction, *International Journal for Numerical Methods in Engineering* 14(9): 1293–1307. http://dx.doi.org/10.1002/nme.1620140904

Kasimov, B. R. 2009. *Issledovanie rosta vnutrennih prodol'nyh treshhin v rel'se v zone vykolov*, in *Aktual'nye Problemy Sovremennyh Nauk – 2009: Internet-Konferenciya*. Available from Internet: http://www.rusnauka.com/17_APSN_2009/Tecnic/48342.doc.htm (in Russian).

Kouroussis, G.; Gazetas, G.; Anastasopoulos, I.; Conti, C.; Verlinden, O. 2011. Discrete modelling of vertical track–soil coupling for vehicle–track dynamics, *Soil Dynamics and Earthquake Engineering* 31(12): 1711–1723. http://dx.doi.org/10.1016/j.soildyn.2011.07.007

Kumar, V.; Rastogi, V. 2009. Investigation of vertical dynamic behaviour and modelling of a typical Indian rail road vehicle through bond graph, *World Journal of Modelling and Simulation* 5(2): 130–138.

Markov, D. P. 2004. Zadir bokovyh poverhnostej rel'sov i grebnej koles, *Vestnik Nauchno-Issledovatel'skogo Instituta Zheleznodorozhnogo Transporta* (4): 40–43. (in Russian).

Newmark, N. M. 1947. Influence charts for computation of vertical displacements in elastic foundations, *University of Illinois Bulletin* 44(45): 1–14. Available from Internet: https://www.ideals.illinois.edu/bitstream/handle/2142/4573/engineeringexperv00000i00367.pdf

Nielsen, J. C. O. 2008. High-frequency vertical wheel–rail contact forces: validation of a prediction model by field testing, *Wear* 265(9–10): 1465–1471. http://dx.doi.org/10.1016/j.wear.2008.02.038

Nielsen, J. C. O.; Abrahamsson, T. J. S. 1992. Coupling of physical and modal components for analysis of moving non-linear dynamic systems on general beam structures, *International Journal for Numerical Methods in Engineering* 33(9): 1843–1859. http://dx.doi.org/10.1002/nme.1620330906

Pieringer, A.; Kropp, W.; Nielsen, J. C. O. 2014. The influence of contact modelling on simulated wheel/rail interaction due to wheel flats, *Wear* 314(1–2): 273–281. http://dx.doi.org/10.1016/j.wear.2013.12.005

Polach, O. 2000. A fast wheel–rail forces calculation computer code, in *The Dynamics of Vehicles on Roads and on Tracks: Proceedings of the 16th IAVSD Symposium*, 30 August – 3 September 1999, Pretoria, South Africa, 728–739.

Pombo, J.; Ambrósio, J.; Silva, M. 2007. A new wheel–rail contact model for railway dynamics, *Vehicle System Dynamics* 45(2): 165–189. http://dx.doi.org/10.1080/00423110600996017

Recuero, A. M.; Escalona, J. L.; Shabana, A. A. 2011. Finite-element analysis of unsupported sleepers using three-dimensional wheel–rail contact formulation, *Proceedings of the Institution of Mechanical Engineers, Part K: Journal of Multi-body Dynamics* 225(2): 153–165. http://dx.doi.org/10.1177/2041306810394971

Sackfield, A.; Dini, D.; Hills, D. A. 2007. Contact of a rotating wheel with a flat, *International Journal of Solids and Structures* 44(10): 3304–3316. http://dx.doi.org/10.1016/j.ijsolstr.2006.09.025

Sackfield, A.; Dini, D.; Hills, D. A. 2006. The contact problem for a wheel having a 'flat', *Wear* 261(11–12): 1265–1270. http://dx.doi.org/10.1016/j.wear.2006.03.009

Sun, Y. Q.; Dhanasekar, M.; Roach, D. 2003. A three-dimensional model for the lateral and vertical dynamics of wagon-track systems, *Proceedings of the Institution of Mechanical Engineers, Part F: Journal of Rail and Rapid Transit* 217(1): 31–45. http://dx.doi.org/10.1243/095440903762727339

Torstensson, P. T; Nielsen, J. C. O.; Baeza, L. 2011. Dynamic train–track interaction at high vehicle speeds: modelling of wheelset dynamics and wheel rotation, *Journal of Sound and Vibration* 330(22): 5309–5321. http://dx.doi.org/10.1016/j.jsv.2011.05.030

Uzzal, R. U. A. 2012. *Analysis of a Three-Dimensional Railway Vehicle-Track System and Development of a Smart Wheelset:* A Thesis in the Department of Mechanical and Industrial Engineering Presented in Partial Fulfillment of the Requirements for the Degree of Doctor of Philosophy at Concordia University. Montreal, Quebec, Canada. 293 p. Available from Internet: http://spectrum.library.concordia.ca/973753

Uzzal, R. U. A.; Stiharu, I.; Ahmed, W. 2009. Design and Analysis of MEMS based accelerometer for automatic detection of railway wheel flat, *World Academy of Science, Engineering and Technology, International Science Index* 3(5): 785–793.

Wang, K. Y.; Liu, P. F.; Zhai, W. M.; Huang, C.; Chen, Z. G.; Gao, J. M. 2015. Wheel/rail dynamic interaction due to excitation of rail corrugation in high-speed railway, *Science China Technological Sciences* 58(2): 226–235. http://dx.doi.org/10.1007/s11431-014-5633-y

Wasiwitono, U.; Zheng, D.; Chiu, W. K. 2007. How useful is track acceleration for monitoring impact loads generated by wheel defects?, in *Proceedings of the 5th Australasian Congress on Applied Mechanics (ACAM 2007)*, 10–12 December 2007, Brisbane, Australia, 502–507.

Wu, T. X.; Thompson, D. J. 2001. *A Hybrid Model for Wheel/Track Dynamic Interaction and Noise Generation due to Wheel Flats*. ISVR Technical Memorandum No. 859. 47 p. Available from Internet: http://resource.isvr.soton.ac.uk/staff/pubs/PubPDFs/Pub1127.pdf

Yazykov, V. N. 2004. *Primenenie modeli negercevskogo kontakta kolesa s rel'som dlya ocenki dinamicheskih kachestv gruzovogo teplovoza*: Dissertaciya na soiskanie uchenoj stepeni kandidata tehnicheskih nauk. Bryansk: Bryanskij gosudarstvennyj tehnicheskij universitet, 151 s. (in Russian).

Zhu, J. J.; Ahmed, A. K. W.; Rakheja, S. 2007. Adaptive contact model for simulation of wheel–rail impact load due to a wheel flat, in *Proceedings of the 13th National Conference on Mechanisms and Machines (NaCoMM07)*, 12–13 December 2007, Bangalore, India, 157–164.

APPENDIX 1

Mass matrices of the ballast and sub-ballast block and a part of the rail:

$$\left[M_{i,j}\right]=diag\left(\left[M_{bi,bi}\right]\ \left[M_{bj,bj}\right]\ \left[M_{Rij,Rij}\right]\right),\quad (A.1.1)$$

where: $\left[M_{bi,bi}\right]$, $\left[M_{bj,bj}\right]$, $\left[M_{Rij,Rij}\right]$ are the blocks of the mass matrix of sub-ballast and a part of the rail:

$$\left[M_{bi,bi}\right]=diag\left(m_{sl,i}\quad m_{s1,i}\quad m_{s2,i}\quad m_{s3,i}\right);$$

$$\left[M_{bj,bj}\right]=diag\left(m_{sl,j}\quad m_{s1,j}\quad m_{s2,j}\quad m_{s3,j}\right);$$

$$\left[M_{Rij,Rij}\right]=diag\left(m_{R,i}\quad m_{R,j}\right).$$

Damping coefficients of sub-ballast and a part of the rail:

$$\left[C_{i,j}\right]=\begin{bmatrix}C_{bi,bi} & C_{bi,bj} & C_{bi,Rij}\\ C_{bj,bi} & C_{bj,bj} & C_{bj,Rij}\\ C_{Rij,bi} & C_{Rij,bj} & C_{Rij,Rij}\end{bmatrix},\quad (A.1.2)$$

where: $\left[C_{bi,bi}\right]$, $\left[C_{bj,bi}\right]$, $\left[C_{Rij,bi}\right]$, $\left[C_{bi,bj}\right]$, $\left[C_{bj,bj}\right]$, $\left[C_{Rij,bj}\right]$, $\left[C_{bi,Rij}\right]$, $\left[C_{bj,Rij}\right]$, $\left[C_{Rij,Rij}\right]$ are the blocks of the damping matrix of sub-ballast and a part of the rail:

$$\left[C_{bj,bj}\right]=\left[C_{bi,bj}\right]^T;$$

$$\left[C_{Rij,bi}\right]=\left[C_{bi,Rij}\right]^T;$$

$$\left[C_{Rij,bj}\right]=\left[C_{bj,Rij}\right]^T.$$

Stiffness coefficients of sub-ballast and a part of the rail:

$$\left[K_{i,j}\right]=\begin{bmatrix}K_{bi,bi} & K_{bi,bj} & K_{bi,Rij}\\ K_{bj,bi} & K_{bj,bj} & K_{bj,Rij}\\ K_{Rij,bi} & K_{Rij,bj} & K_{Rij,Rij}\end{bmatrix},\quad (A.1.3)$$

where: $\left[K_{bi,bi}\right]$, $\left[K_{bj,bi}\right]$, $\left[K_{Rij,bi}\right]$, $\left[K_{bi,bj}\right]$, $\left[K_{bj,bj}\right]$, $\left[K_{Rij,bj}\right]$, $\left[K_{bi,Rij}\right]$, $\left[K_{bj,Rij}\right]$, $\left[K_{Rij,Rij}\right]$ are the blocks of the stiffness matrix of sub-ballast and a part of the rail:

$$\left[K_{bj,bj}\right]=\left[K_{bi,bj}\right]^T;$$

$$\left[K_{Rij,bi}\right]=\left[K_{bi,Rij}\right]^T;$$

$$\left[K_{Rij,bj}\right]=\left[K_{bj,Rij}\right]^T.$$

Load force vectors:

$$\left\{F_{b,i,j}\right\}^T=\left[\left\{F_{bi}\right\}^T\ \left\{F_{bj}\right\}^T\ \left\{F_{Rij}\right\}^T\right],$$

where: $\left\{F_{bi}\right\}$, $\left\{F_{bj}\right\}$, $\left\{F_{Rij}\right\}$ are vectors in the points i and j of load forces.

APPENDIX 2

The mass of the railway vehicle:

$$\left[M_{RB}\right] = diag\left(m_{bg1}\ m_{bg2}\ m_{bg3}\ m_{bg4}\right), \qquad \text{(A.2.1)}$$

where: m_{bg1}, m_{bg2}, m_{bg3}, m_{bg4} are the masses of the vehicle.

Damping and stiffness matrices of the vehicle:

$$\left[C_{bg}\right] = \begin{bmatrix} c_{bg12} & -c_{bg12} & 0 & 0 \\ -c_{bg12} & c_{bg12}+c_{bg23} & -c_{bg23} & 0 \\ 0 & -c_{bg23} & c_{bg23}+c_{bg34} & -c_{bg34} \\ 0 & 0 & -c_{bg34} & c_{bg34} \end{bmatrix}; \qquad \text{(A.2.2)}$$

$$\left[K_{bg}\right] = \begin{bmatrix} k_{bg12} & -k_{bg12} & 0 & 0 \\ -k_{bg12} & k_{bg12}+k_{bg23} & -k_{bg23} & 0 \\ 0 & -k_{bg23} & k_{bg23}+k_{bg34} & -k_{bg34} \\ 0 & 0 & -k_{bg34} & k_{bg34} \end{bmatrix}, \qquad \text{(A.2.3)}$$

where: k_{bg12}, k_{bg23}, k_{bg34} and c_{bg12}, c_{bg23}, c_{bg34} are damping and stiffness coefficients of vehicle elements.

Weight force vector of the railway vehicle:

$$\left\{F_{bg}\left(t\right)\right\} = \left[-m_{bg1}g\ -m_{bg2}g\ -m_{bg3}g\ -m_{bg4}g\right]. \qquad \text{(A.2.4)}$$